

Drop size ambiguities in the retrieval of precipitation profiles from dual-frequency radar measurements

Jonathan P. Meagher¹, Ziad S. Haddad^{1,3}, Stephen L. Durden¹, Eric A. Smith²
and Eastwood Im¹

Abstract

The Tropical Rainfall Measuring Mission experience has confirmed that one of the main difficulties in retrieving rain profiles from single-frequency radar reflectivity measurements is the unknown raindrop size distribution (DSD). A dual-frequency radar such as the one planned for the up-coming Global Precipitation Measurement (GPM) core satellite is expected to help sort out at least part of this DSD-induced ambiguity. However, the signature of precipitation at 14 GHz does not differ greatly from its signature at 35 GHz (the GPM radar frequencies). In order to determine the extent of the vertical variability of the DSD in tropical systems and to quantify the effectiveness of a dual-frequency radar in resolving this ambiguity, we consider several different models of DSD shape, and use them to estimate the rain-rate and mean-diameter profiles from the measurements made by JPL's airborne PR-2 radar over hurricanes Gabrielle and Humberto during the CAMEX-4 experiment in September 2001. It turns out that the vertical structures of the rain profiles retrieved from the same measurements under different DSD assumptions are similar, but the profiles themselves are quantitatively significantly different.

30th September 2003

¹Jet Propulsion Laboratory, California Institute of Technology

²NASA Goddard Space Flight Center

³Corresponding author: 300-243 JPL, Pasadena CA 91109-8099 – zsh@albertoVO5.jpl.nasa.gov

I. INTRODUCTION

The rain-profiling algorithm development and validation effort undertaken for the Tropical Rainfall Measuring Mission has confirmed that one of the main difficulties surrounding the retrieval of rain rate profiles from spaceborne radar reflectivity measurements is the unknown drop size distribution (DSD). Indeed, if one starts with the assumption that the DSD is always an exponential (or, at worst, a gamma) distribution, whose dependence on the rain rate is known a priori, one can then derive power-law relations $Z = aR^b$ and $k = \alpha R^\beta$ which very adequately relate the 14-GHz radar reflectivity factor Z and the 14-GHz attenuation coefficient k to the rain rate R . It follows (see e.g. Haddad et al, 1995) that the one-way path-integrated attenuation PIA , integrated over a vertical rain column, must be related to the 14-GHz measured reflectivities Z_m in that column by

$$PIA = \left(1 - 0.2 \log(10) \alpha \frac{\beta}{b} \int (Z_m/a)^{\beta/b} \right)^{b/\beta} \quad (1)$$

Figure 1 is a plot of the PIA values obtained from the TRMM radar measurements over the ocean during several orbits by comparing the rainy surface return with the average surface return from the nearby clear-air regions. This “surface-reference” PIA is shown on the horizontal axis, while the vertical axis represents the right-hand-side of (1) calculated with two different DSD assumptions (corresponding to a few different sets of constant a , b , α and β). The left panel shows the result of using the a-priori values of the parameters a , b , α and β in the TRMM radar algorithm (Iguchi et al, 2000); the right panel shows the result of using those parameters in the multiple-DSD TRMM combined radar/radiometer algorithm (Haddad et al, 1997a) which produce the largest attenuation. If (1) were verified exactly, one would expect much less scatter than is evident in the plots. Indeed,

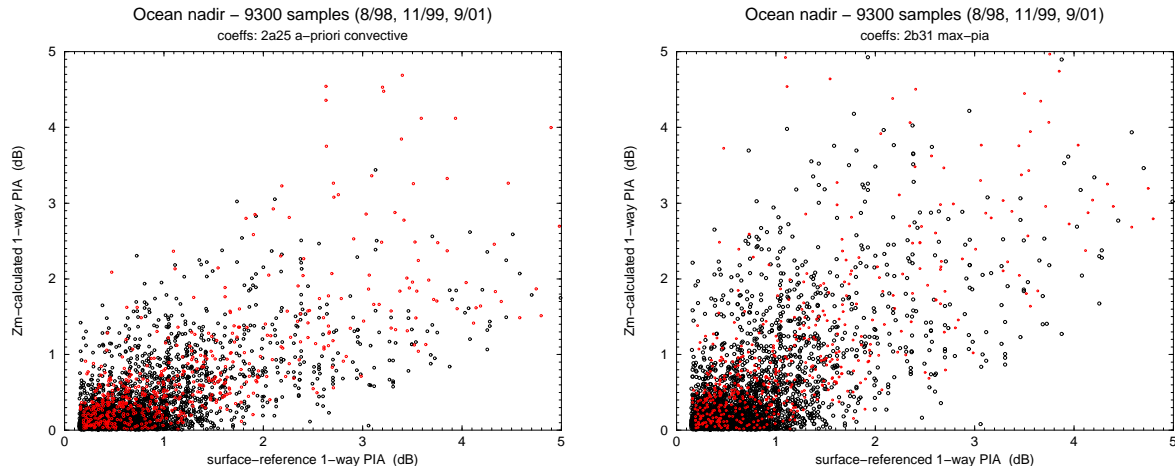


Fig. 1. Z_m -derived PIA versus surface-reference estimates from the TRMM data: poor correlation at moderate and low precipitation.

for one-way attenuations below 1.5 dB, there does not seem to be any correlation between the two sides of (1), though there is a clear tendency for the Z-calculated values to be much smaller than the surface-referenced ones. This apparent failure of equation (1) is quite possibly caused in part to the change in the surface backscattering cross-section due to the variation of the wind from the clear air regions to the rainy area. But this effect is not sufficient to explain the large mismatch at moderate and low precipitation. Indeed, this discrepancy constitutes compelling evidence that the DSD parameters vary very significantly over a rain column.

In the case of TRMM, this DSD problem has been dealt with in two ways. In the radar algorithm, (1) is used to adjust the ratio $\alpha\beta/b$ and thus reduce the ambiguity, at least in the case of heavier precipitation. In the Bayesian framework of the TRMM combined radar/radiometer algorithm, (1) is used to weight the candidate a-priori DSD's in favor of the better-matching ones, and the observed radiances are also used to further constrain the multiple possibilities for the DSD. The dual-frequency radar which the Global Precipitation Measurement (GPM) mission's core satellite will carry should prove a much more effective tool in sorting out at least part of this DSD-induced ambiguity. Indeed, with two radar reflectivity profiles, one would expect to be able to retrieve not just a single rain rate profile, but in addition at least one "first order" DSD profile, e.g. a profile of the (mass-weighted) mean drop diameter D^* . Unfortunately, this expectation may turn out to be difficult to fulfill. That is because the reflectivity profiles at the two radar frequencies are far from independent. After all, lighter rain is made up mostly of small drops. As figure 2 shows, the backscattering cross-section of small drops is not significantly different at 14 and 35 GHz. One would therefore not expect large differences in the associated radar reflectivity factors. While the difference in the extinction cross-section appears more readily exploitable for small drops, its actual magnitude is unfortunately so small that the resulting attenuation is not significant for light precipitation. At the other extreme, while the attenuation will be appreciable (at both frequencies) for heavy rain, it is in fact likely to be so appreciable as to drive the back-scattered 35-GHz signal itself below the sensitivity threshold of that channel. Thus, the two frequencies are not very different at low rain rates, and they will in effect reduce to a single frequency at high rain rates, leaving a somewhat disappointing range over which the two frequencies can be realistically expected to resolve the DSD-induced ambiguity problem. That is why it is at least as important for GPM as it was for TRMM to develop an optimal approach to extract from all the GPM core satellite's measurements profiles of the best unbiased estimates of the means of the rain rate R and mass-weighted mean diameter D^* . The purpose of this paper is to quantify the effect of different plausible a-priori

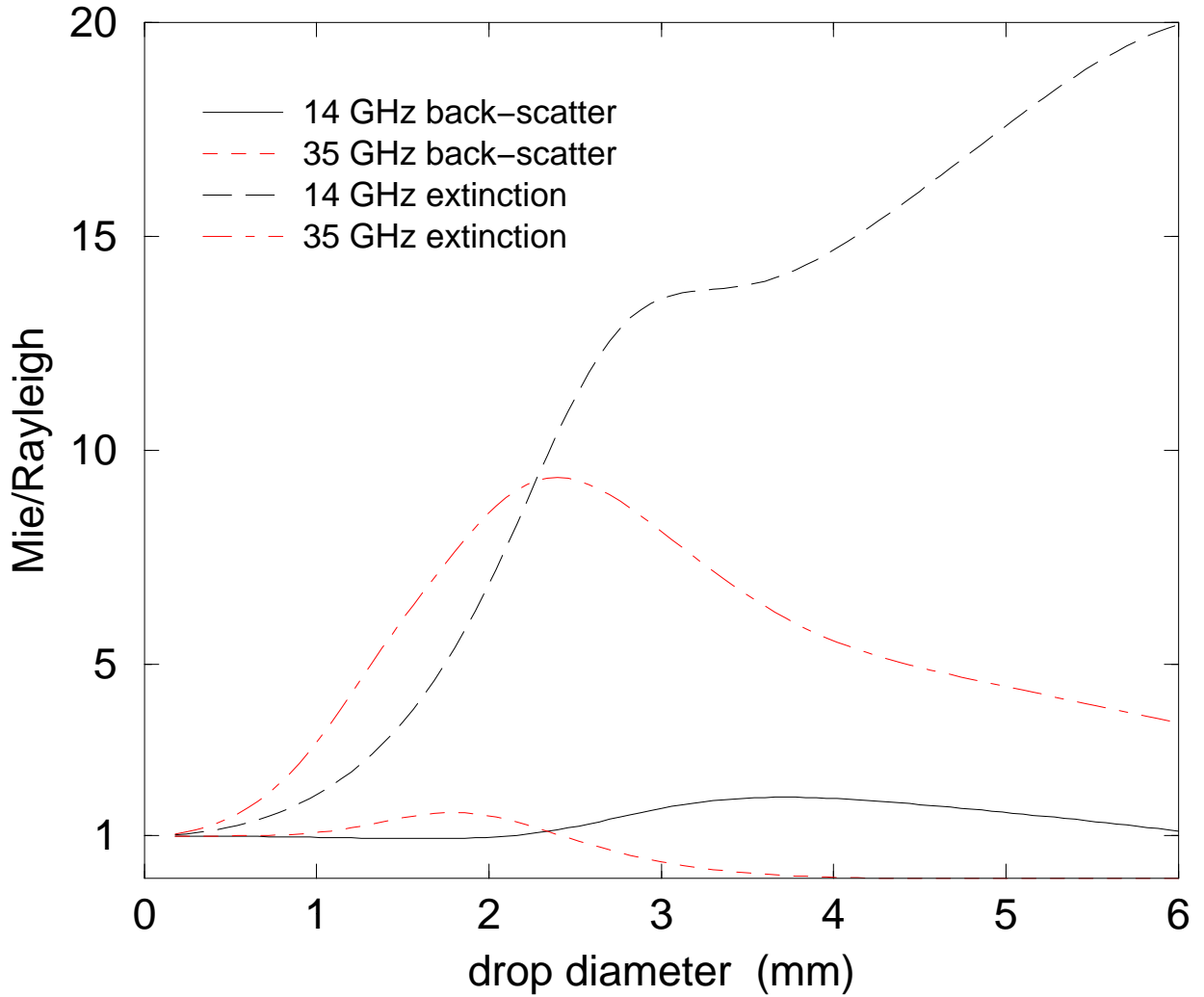


Fig. 2. Actual (*Mie*) vs small-size-approximation (*Rayleigh*) microwave signatures of rain drops.

assumptions about the possible shapes of the DSD on the retrieved precipitation profiles using data from CAMEX-4.

II. DIFFERENT DSD MODELS

We shall consider five well-documented DSD models. No discussion of DSD's can be complete without considering Marshall and Palmer's exponential form (Marshall and Palmer, 1948)

$$N_{MP}(D) = N_0 e^{-\Lambda D} \quad (2)$$

in which, if we assume a nominal terminal fall velocity of $9.56(1 - e^{-0.53D})$ m/s for drops of diameter D mm, the parameters N_0 and Λ must be consistent with R , i.e. must satisfy

$$R = 0.11 \left(\frac{1}{\Lambda^4} - \frac{1}{(\Lambda + 0.53)^4} \right) N_0 \text{ mm/hr} \quad (3)$$

with N_0 in $\text{mm}^{-1} \text{ m}^{-3}$. Thus, in addition to R , the exponential N_{MP} has a single free parameter. As long as equation (3) is enforced, whether one chooses to identify this parameter as N_0 or Λ makes no difference whatever, and we shall choose Λ , with the additional constraint that the ratio $4/\Lambda$, which is equal to the mass-weighted mean drop diameter, not exceed 3 mm. The second, third and fourth DSD models which we consider are special cases of the gamma DSD

$$N_\Gamma(D) = N_0 D^\mu e^{-\Lambda D}. \quad (4)$$

This distribution effectively depends on two parameters in addition to R . There are several ways of constraining one of these parameters to end up with only two unknowns which can be solved for using the two measured radar reflectivity factors. One that has proved consistent with disdrometer and airborne 2D-probe (small-)sample statistics consists in re-expressing μ and Λ in terms of the mass-weighted mean drop diameter D^* and the dimensionless relative mass-weighted r.m.s. diameter deviation s^* , and enforcing on the pair (D^*, s^*) the rather restrictive joint behavior quantified by the sample statistics observed during the TOGA-COARE campaign (Lukas et al, 1995) and during the 1992-1993 Darwin field measurements (Haddad et al, 1997b). Roughly, these restrictions amount to requiring that $D^* R^{-0.155}$ have a mean of about 1.1 (with R in mm/hr and D^* in mm) and a standard deviation of about 0.3, while $s^* D^{*-0.165} R^{-0.011}$, which has a mean of about 0.4 and a tiny standard deviation smaller than 0.05, is fixed at 0.4 so that $D'' = D^* R^{-0.155}$ is the independent DSD parameters in this case. We shall refer to the resulting “restricted” gamma DSD model as N_{Γ_0} . This is the second DSD which we shall consider. It is the one used in the TRMM combined radar/radiometer algorithm. The third and fourth DSD models are similar restrictions of the gamma model, obtained from (4) by imposing a deterministic relation between N_0 and μ . We chose the relation (Ulbrich and Atlas, 1998)

$$N_0 = 6734 \cdot e^{1.45\mu} \text{ mm}^{-1-\mu} \text{ m}^{-3} \quad (5)$$

for the third model N_{Γ_1} , and the relation (Ulbrich, 1983)

$$N_0 = 1500 \cdot e^{0.84\mu} \text{ mm}^{-1-\mu} \text{ m}^{-3} \quad (6)$$

for the fourth model N_{Γ_2} . Finally, we also consider a model which does not depend on any closed analytic form for the distribution function N . After all, there is an enormous wealth of sampled

DSD's measured from various probes, and there is no reason not to use a large subgroup of such samples as an a-priori database in lieu of a model. Indeed, for our fifth DSD “model” N_C , we chose the TOGA-COARE database of DSD samples collected by the NCAR 2-D PMS probes mounted on the NCAR Electra aircraft over the warm pool of the western equatorial Pacific between November 1992 and February 1993 – an earlier analysis had reduced this dataset using a principal component analysis (Meagher and Haddad, 2002), but while this produced a more efficient way to code the data, the resulting savings in computer resources (memory and processing) are not significant for the current study and we used the original database of DSD samples itself.

The next step is to calculate the Mie extinction and back-scattering efficiencies as a function of drop diameter. Once this is done, one can associate to each rain-rate/DSD pair (R, N) in any one of our five models the corresponding radar reflectivity factors $z_{14}(R, N)$ and $z_{35}(R, N)$ (in $\text{mm}^6 \text{ m}^{-3}$), and the corresponding attenuation coefficients $k_{14}(R, N)$ and $k_{35}(R, N)$ (in dB/km). Figure 3 shows the resulting “reflectivity manifolds” (to borrow a term dear to the passive radiometer community – see e.g. Smith and Mugnai, 1988) for each of our DSD models. In the case of N_{MP} , N_{Γ_0} , N_{Γ_1} and N_{Γ_2} , these manifolds were obtained by choosing a few representative values for the free DSD parameter (Λ in the case of N_{MP} , N_{Γ_1} and N_{Γ_2} , D'' in the case of N_{Γ_0}), and letting R vary from 0.2 to 200 mm/hr. In the case of N_C , the manifold is computed directly from the DSD samples in the database. In all cases, the value of the difference $z_{14}(R, N) - z_{35}(R, N)$ is plotted versus $z_{14}(R, N)$. The first observation is that, for all five DSD models, when the 14-GHz reflectivities are small, the rain rate curves are almost horizontal, confirming our previous observation that for lighter precipitation there is no significant difference between the two frequencies.

There are two additional facts illustrated by the figure which are crucial to the retrieval problem. The first is that all the “curve crossings” correspond to retrieval ambiguities: they indicate that a pair of (14-GHz, 35-GHz) reflectivity factors can be explained by at least two rain rates (which can differ by a factor of two or more – the two-dimensional manifolds could not be readily made to illustrate this ambiguity quantitatively), associated to different DSD parameter values. This implies that even in the absence of any observation noise, the dual-frequency retrieval problem can be ambiguous, and manifestly more so in the case of N_{MP} than in the other cases, though all the models have non-negligible ambiguities at low precipitation. Since these ambiguities are intrinsic to the dual-frequency observations, one would need to consider additional measurements to resolve them. The second point concerns the “blank” regions in the plots. These are most evident in the least ambiguous cases N_{Γ_0} and N_{Γ_1} , though they are not entirely absent in the other models.

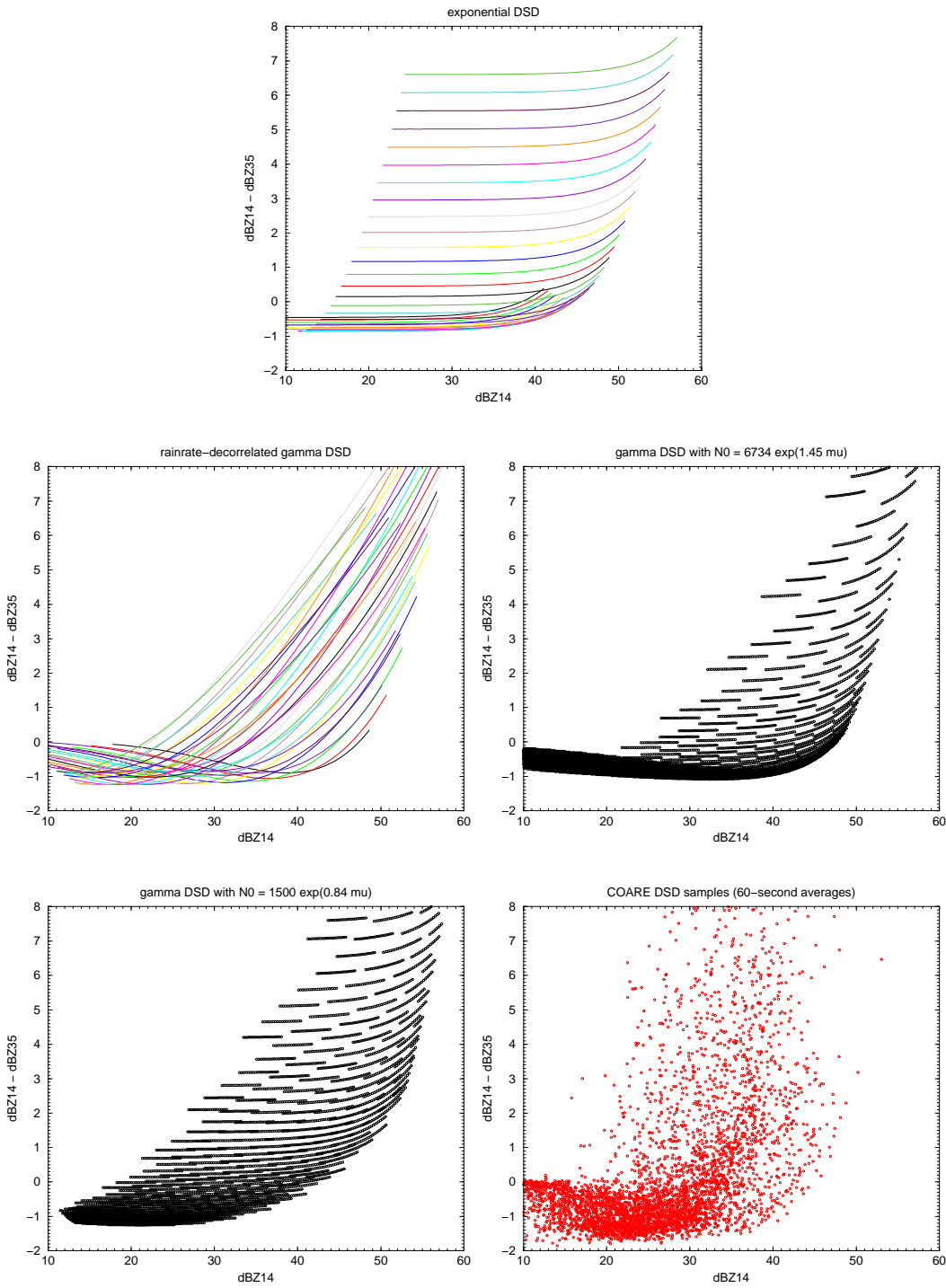


Fig. 3. Reflectivity “manifolds” ($z_{14} - z_{35}$) vs z_{14} for the DSD’s N_{MP} (top), N_{Γ_0} (middle left), N_{Γ_1} (middle right), N_{Γ_2} (lower left), and N_C (lower right), showing the rain rate flow lines (i.e. each curve corresponds to a fixed value of the free parameter of the respective DSD)

Indeed, current technology cannot guarantee that the noise in the reflectivity measurements is less than about 0.3 dB r.m.s. at best. Thus, one's actual observations could quite easily fall outside the region covered by our manifolds, i.e. it is quite likely that with any DSD model one will face the situation where no rain rate can “explain” exactly a pair of (noisy) reflectivities. Therefore, when attempting a retrieval, one must have a rigorous mechanism to assess the plausibility of the various model pairs which are “close” to the measured pair. In summary, a dual-frequency radar cannot entirely avoid the ambiguities with which we have been all too familiar in the case of the TRMM radar, and the noise in the measurements (along with the unavoidable imperfection of any DSD model) will make it essential to allow for multiple inexact “matches”. Both of these concerns make it highly desirable to use a Bayesian framework to make unbiased estimates of the precipitation underlying the measurements.

There is yet another problem which leads us to consider a sixth case. It is brought about by the need to account for the cumulative attenuation at both frequencies as one estimates the rain rate sequentially through the consecutive vertical range bins in the cloud. It is however easiest to describe this sixth case once the retrieval approach has been outlined, in the following section.

III. DUAL-FREQUENCY BAYESIAN RETRIEVAL

In order to keep the problems associated with the specific retrieval procedure separate from the DSD ambiguities themselves, we applied the simplest Bayesian approach to the dual-frequency profiling problem. Let us start by fixing the notation. For a given vertical column of precipitation, call $Z_{14}(i)$ (respectively $Z_{35}(i)$) the radar reflectivity factor measured from the i^{th} vertical range bin at 14 (resp. 35) GHz, with $i = 1$ for the first bin at the top of the rainy cloud and increasing downward. The equations that have to be solved for the rain-rate/DSD pair (R, N) at each range bin i are

$$Z_{14}(i) = z_{14}(R, N) - 2A_{14}(i-1) + \text{noise}_{14} \quad (7)$$

$$Z_{35}(i) = z_{35}(R, N) - 2A_{35}(i-1) + \text{noise}_{35} \quad (8)$$

where $A_{14}(i-1)$ (resp. $A_{35}(i-1)$) is the one-way 14 (resp. 35) GHz attenuation accumulated from the top of the cloud until the i^{th} range bin, expressed in dB. To solve equations (7)-(8) for the unknowns R and N , one would thus need to track the accumulated attenuations A_{14} and A_{35} . Assuming that the noise terms “ noise_{14} ” and “ noise_{35} ” are 0-mean Gaussian with variances σ_{14}^2 and σ_{35}^2 , the simplest Bayesian approach consists in two steps repeated recursively for the consecutive range bins:

1. starting at the top of the cloud ($i = 1$), and setting $A_{14}(0) = A_{35}(0) = 0$, consider all realistic rain rates R and all DSD's N allowed by the a-priori model, and calculate for each pair (R, N) its mean-squared distance d_i from the two independent measurements:

$$d_i(R, N) = \left(\frac{[Z_{14}(i) + 2A_{14}(i-1)] - z_{14}(R, N)}{\sigma_{14}} \right)^2 + \left(\frac{[Z_{35}(i) + 2A_{35}(i-1)] - z_{35}(R, N)}{\sigma_{35}} \right)^2 \quad (9)$$

The optimal unbiased estimate of the rain rate would then have to be given by

$$\hat{R}(i) = \sum_N \int R p_i(R, N) dR \quad (10)$$

where p_i is the probability weight $p_i(R, N) = e^{-0.5d_i(R, N)}$, normalized so that $\sum \int p_i = 1$.

2. the corresponding accumulated attenuation up to and including the current range bin must then be updated, using the similar formula

$$A_f(i) = A_f(i-1) + \sum_N \int \delta k_f(R, N) p_i(R, N) dR \quad (11)$$

where δ is the thickness of the range bin (in km), and $f = 14$ or 35 GHz.

This is the Bayesian retrieval approach which we used.

Before illustrating this method and comparing its retrievals with the five a-priori DSD cases, we shall now describe a sixth case which we had to consider for completeness. It comes about because equations (7)-(8) are not exactly correct. Indeed, rain is not the only source of attenuation of microwaves in the atmosphere. While absorption by oxygen and water vapor is relatively small and largely predictable, the attenuation due to cloud liquid water, especially at 35 GHz, is not negligible. That is because the downward-looking radar will measure

$$Z(i) = \int \int \left(\int_{(i-1)\delta}^{i\delta} z(r, \theta, \phi) e^{-\int_r^{top} k(r', \theta, \phi) dr'} dr \right) d\theta d\phi \quad (12)$$

and while z in the right-hand-side is the radar reflectivity factor of the rain, the attenuation coefficient k is the sum $k_{rain} + k_{cloud}$ of the attenuations due to the precipitation and to the cloud (the reflectivity of the cloud droplets is negligible because it is proportional to the sixth power of the droplet diameter). At 35 GHz, if M is the cloud liquid water content in g/m^3 , $k_{cloud} \simeq \kappa M$ dB/km, with $\kappa = 0.84 \text{ m}^3 \text{ g}^{-1} \text{ dB km}^{-1}$ when all cloud droplets are $10 \mu\text{m}$ in diameter (and κ increases toward a value of 1.4 when all drops approach drizzle size). Thus, while the cloud is not sufficiently reflective to be detectable, it will cast a “shadow”, and this shadow may differ in “clear air” and

within the rain. For example, a rather moderate two vertical kilometers of liquid cloud carrying 0.5 g/m^3 of water will attenuate the 35 GHz signal by about 1 dB. This presents two problems. First, the surface cross-section in “clear air” (i.e. where the reflectivities from the atmosphere do not exceed the relatively high radar noise threshold), which is necessary to the proper estimation of the integrated attenuation within precipitation, would be under-estimated if no account is taken of the attenuation due to any undetected cloud. This would result in an underestimate of the PIA, and that is the main reason we chose not to use any a-priori information about the PIA in our retrieval approach. Second, within the precipitation, at each vertical resolution bin one must estimate (and “remove”) the attenuation in the left-hand-side of (12), and this cannot be done without biasing the estimate if one does not know how to apportion the attenuation between precipitating and non-precipitating liquid. We decided to test the effect of this “cloud-shadow” problem by considering a sixth case, where the DSD is the TOGA-COARE database of N_C ’s as in the fifth DSD model, but where we systematically assume the existence of cloud liquid with liquid water content M (g/m^3) equal to 20% of the precipitating liquid water in the given DSD sample and with an attenuation coefficient of $0.84 M \text{ dB/km}$. We shall refer to this DSD case as N_{CC} .

To verify the accuracy of this dual-frequency Bayesian approach, it was tested on synthetic “data” which was constructed as follows. Starting with the rain-rate profiles obtained from the single-frequency TRMM radar algorithm over hurricane Bonnie on August 22, 1998, we super-imposed the DSD model N_{Γ_0} with various values of the parameter D'' , making sure to vary D'' in all three spatial dimensions. We then (re-)synthesized “measured” reflectivity profiles Z_{14} and Z_{35} at the TRMM resolution but assuming sensitivity thresholds of 17 dBZ at 14 GHz and 15 dBZ at 35 GHz. We then applied the Bayesian approach described above to verify that the estimates do match the original rain rates and the super-imposed values of D'' . The results are illustrated in figure 4, which shows estimated versus original rain rates, grouped into two “seasons”, one consisting of profiles where the values of D'' in the super-imposed DSD were low (the “low-D season”) and one where the value of D'' were large (the “high-D season”). For comparison, single-frequency (14 GHz) retrievals are also shown. The scatter in the dual-frequency Bayesian retrieval did increase substantially below 1 mm/hr and above 12 mm/hr, but that was expected since at low rain rates the second frequency simply adds no independent information and at high rain rates the significant 35-Ghz attenuation forces the 35-GHz echo below the assumed sensitivity threshold. Thus one can conclude that the Bayesian dual-frequency approach performs quite satisfactorily.

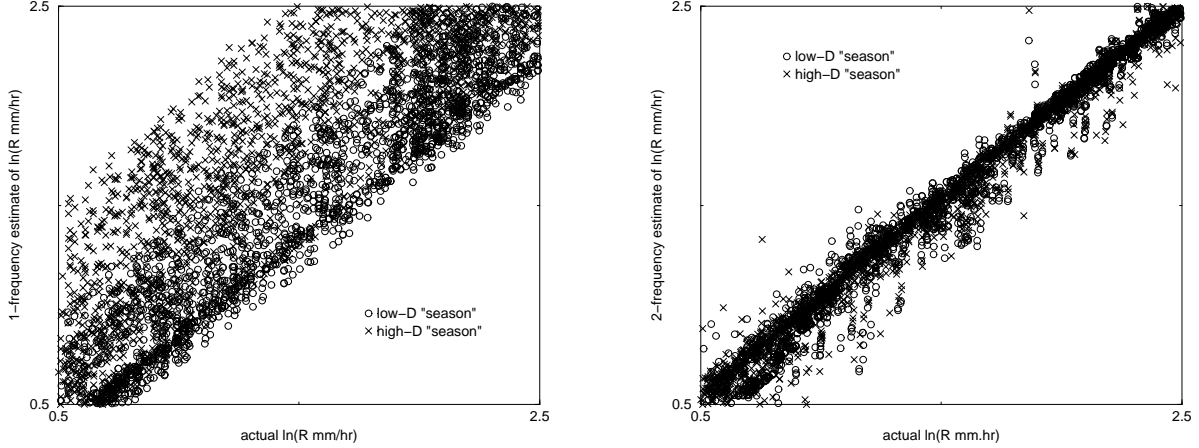


Fig. 4. Estimated versus original rain rates, with small-drop cases indicated with an \times , the large-drop cases indicated with a \circ . The left panel shows the single-frequency retrievals, which mis-interpret the changing DSD, resulting in biased estimates. The right panel shows the dual-frequency Bayesian estimates.

IV. THE CAMEX-4 RESULTS

We are now ready to apply the retrieval procedure outlined above to the data collected by JPL's airborne PR-2 radar over tropical storm Gabrielle and Hurricane Humberto during the CAMEX-4 experiment. Figures 5 through 8 show the results of the retrievals. The top two panels of figure 5 show the rather low radar reflectivities measured at nadir over Tropical Storm Gabrielle on September 15, 2001. The system had just emerged off the Florida coast over the Gulf Stream (around 30°N 79°W), but had not re-intensified. The remaining panels of figure 5 show the retrieved rain rates and mean drop diameters for each of the DSD models N_{MP} , N_{Γ_0} , N_C and N_{CC} . The top panels of figure 6 show the one-way integrated attenuations corresponding to each of the models considered, along with the surface-reference PIA estimated from two models: a single average clear-air surface-cross-section reference value, and a fitted model as in Li et al, 2002. The remaining panels of figure 6 show the difference between the measured radar reflectivity factors and those reconstructed from the results of the Bayesian retrieval, in each of the four cases considered in this example. The top two panels of figure 7 show the radar reflectivities measured at nadir over Hurricane Humberto on September 24, 2001. The cyclone was embedded in a strong southwesterly flow, and anticyclonic outflow from the convective region was quite obvious. The warm core in the eye was weak, about 2 to 3 K warmer than the surrounding environment. There was a large cirrus outflow extending several hundred nautical miles from the center near 37°N 63°W . The remaining panels in figure 7 show the retrieved rain rates and mean drop diameters for each of the DSD models N_{MP} , N_{Γ_0} , N_{Γ_1} , N_{Γ_2} , and N_C . Finally, the top panels of figure 8 show the various

PIA's, and the remaining panels of figure 8 show the errors in the case of N_{MP} , N_{Γ_0} and N_C .

The reflectivities measured in Gabrielle never exceeded about 40 dBZ, and at no time was the 35-GHz echo attenuated below the sensitivity threshold of the radar. Figure 5 shows that the retrieved vertical structure of the precipitation is quite similar in all four cases considered. The exponential model MP produces unrealistically large rain rates in the three convective regions (near km 220, km 270 and km 350), and very large mean hydrometeor sizes above the freezing level. Figure 6 confirms that the error in all four models is quite low, except within the melting layer in the restricted-gamma case N_{Γ_0} , where the model manifestly cannot explain the measured reflectivities without errors of about 2 dB. In general, the errors are lowest in the case of N_C and N_{CC} . A quantitative comparison of the estimates obtained using the various DSD models reveals significant differences between N_{MP} on one hand and the three other models on the other hand. Indeed, the average vertical rain rate profile estimated using any of the DSD models except the exponential is between 2 and 3 mm/hr (with the exponential DSD model, the average rain rate increases rapidly from about 1 mm/hr at 4km to 11 mm/hr near at surface). Similarly, except in the exponential case, the average vertical mean-drop-size profile increases from the top to a value near 1.4 mm in the melting layer, then remains near 1.2 mm from 4 km down to the surface (with the exponential DSD model, the average mean-drop-size reaches 1.8 mm in the melting layer, drops to about 0.9 mm at 4 km altitude, and remains fairly constant down to the surface). As to the cloud-attenuation effect, the rain-rate estimates obtained using the rain+cloud model N_{CC} are very close to those of the rain-only model N_C aloft, though as the altitude decreases the rain rates estimated using the rain+cloud model increase steadily with respect to those of the rain-only model, the increase reaching about 50% near the surface. However, remarkably, the mean drop size estimated by the rain+cloud and the rain-only models are almost identical.

In the case of Humberto, figure 7 clearly several cells with significant convection, and in fact the 35-GHz echo disappears at several locations along the track, most notably near km 110 and between km 170 and km 210. The vertical structure of the retrieved rain rates and mean drop sizes from all the models except the exponential are quite similar. The latter was manifestly ill-suited to explain the measurements in this case and figure 8 confirms that its errors are not negligible. This figure also shows that the models N_{Γ_0} , N_{Γ_1} and N_{Γ_2} (as well as N_{MP}) fail whenever the 35-GHz is attenuated into the noise, but the raw-samples model N_C produces remarkably low errors even when the 35-GHz channel is attenuated into noise. A quantitative comparison of the differences

in the estimates due to the different DSD models confirms that the exponential model is the least consistent with the measurements, the database model is the most consistent, and the restricted gamma models fall in between. Specifically, the average vertical rain rate profile in the case of N_{Γ_2} and N_C increases from about 4 mm/hr at 4 km to about 10.5 mm/hr near the surface; in the case of N_{Γ_0} , it increases from about 5 mm/hr at 4 km to a rather large 40 mm/hr near the surface; and in the case of N_{MP} and N_{Γ_1} , it increases from about 6 mm/hr at 4 km to a rather unrealistic 90 mm/hr near the surface. As to the average mean drop size, the estimates obtained using N_{Γ_0} and N_C are very close, remaining near 1.5 mm from 3.5 km down to the surface; the mean drop size in the case of N_{Γ_2} remains near 1.7 mm from the melting layer down to the surface; and the mean drop size in the case of N_{Γ_1} is systematically the lowest, increasing from 1.2 mm just below the melting layer to 1.5 mm near the surface.

Most interesting, all the DSD models (except the exponential) produce rain-rate and mean-drop-size estimates which are very significantly correlated. This is illustrated in figures 9 and 10. In the three restricted-gamma models, the joint behavior of the mean-drop-size and the rain-rate is approximately bimodal, clustering around the “upper” and “lower” log-linear $D^* - R$ relations given in the following table:

DSD model	high- D^* relation	low- D^* relation
Γ_0	$D^* = 1.42R^{0.15}$	$D^* = R^{0.044}$
Γ_1	$D^* = 1.1R^{0.17}$	$D^* = 0.91R^{0.06}$
Γ_2	$D^* = 1.45R^{0.19}$	$D^* = 1.31R^{0.066}$

with R in mm/hr and D^* in mm. In the database case, the estimates cluster around the piecewise log-linear relation

$$D^* = 0.95R^{0.2} \text{ if } R < 7.4 \quad (13)$$

$$= 1.22R^{0.075} \text{ if } R > 7.4 \quad (14)$$

The particularly striking fact is that for heavier rain (R greater than about 10 mm/hr), the estimates overwhelmingly cluster around the “low- D^* ” correlation curves, in all four cases. This would imply that the mean drop size at high rain rates is smaller than one would anticipate from correlation models derived from more moderate precipitation. Similarly, for lighter rain, while there is no pronounced trend in the restricted-gamma models, the estimates produced by the COARE-database DSD model do cluster around a $\log(D^*) - \log(R)$ curve with a steeper slope than the one obtained

at higher rain rates, implying that the mean drop size decreases more rapidly with decreasing rain rate when the latter falls below about 4.5 mm/hr. This supports the likelihood that the mean drop size at lighter precipitation is indeed smaller than one might anticipate from a correlation model derived from more intense precipitation.

The main conclusion of this analysis has to be that several quite different DSD models do indeed produce plausible dual-frequency precipitation estimates, at least over tropical systems like those observed during CAMEX-4. The general shape of the vertical variation of the retrieved rain rates and mean drop sizes will be similar among the different models, but the precipitation amounts and the actual profiles of mean drop diameter differ from model to model, as do the resulting correlation patterns between rain rate and mean drop diameter. The most important implication is that the decision about which drop size distributions should be considered a-priori plausible does have a determining effect on the eventual retrievals. It is therefore very important to justify such a-priori assumptions with detailed DSD measurements at radar-sized resolutions.

Acknowledgment:

This work was performed at the Jet Propulsion Laboratory, California Institute of Technology, under contract with the National Aeronautics and Space Administration.

References:

Z.S. Haddad, E.A. Smith, C.D. Kummerow, T. Iguchi, M.R. Farrar, S.L. Durden, M. Alves and W.S. Olson, 1997a: “The TRMM ‘Day-1’ radar/radiometer combined rain-profiling algorithm”, *J. Met. Soc. Japan*, vol. 75, 799-809.

Z.S. Haddad, D.A. Short, S.L. Durden, E. Im, S. Hensley, M.B. Grable and R.A. Black, 1997b: “A new parametrization of the rain drop size distribution”, *I.E.E.E. Trans. Geosci. Remote Sensing*, vol. 35, 532-539.

Z.S. Haddad, A.R. Jameson, E. Im and S.L. Durden, 1995: “Improved coupled Z-R and k-R relations and the resulting ambiguities in the determination of the vertical distribution of rain from the radar backscatter and the integrated attenuation”, *J. App. Meteor.*, vol. 34, 2680-2688.

T. Iguchi, T. Kozu, R. Meneghini, J. Awaka and K. Okamoto, 2000: “Rain-profiling algorithm for the TRMM precipitation radar”, *J. App. Meteor.*, vol. 39, 2038-2052.

L. Li, E. Im, S.L. Durden and Z.S. Haddad, 2002: “A surface wind model-based method to estimate rain-induced radar path attenuation over ocean”, *J. Atmos. Ocean. Tech.*, vol. 19, 658-672.

R. Lukas, P.J. Webster, M. Ji and A. Leetmaa, 1995: “The large-scale context of the TOGA Coupled Ocean Atmosphere Response Experiment”, *Met. Atmos. Phys.*, vol. 56, 3-16.

J.S. Marshall and W.M.K. Palmer, 1948: “The distribution of rain drops with size”, *J. Meteor.*, vol. 5, 165-166.

J.P. Meagher and Z.S. Haddad, 2002: “Principal-component analysis for raindrops and its application to the remote sensing of rain”, *Q. J. Roy. Met. Soc.*, vol. 128, 559-571.

E.A. Smith and A. Mugnai, 1988: “Radiative transfer to space through a precipitating cloud at multiple microwave frequencies II: results and analysis”, *J. Appl. Meteor.*, vol. 27, 1074-1091.

C.W. Ulbrich and D. Atlas, 1998: “Rainfall microphysics and radar properties: analysis methods for drop size spectra”, *J. Appl. Meteor.*, vol. 37, 912-923.

C.W. Ulbrich, 1983: “Natural variations in the analytical form of the raindrop size distribution”, *J. Clim. Appl. Met.*, vol. 22, 1764-1775.

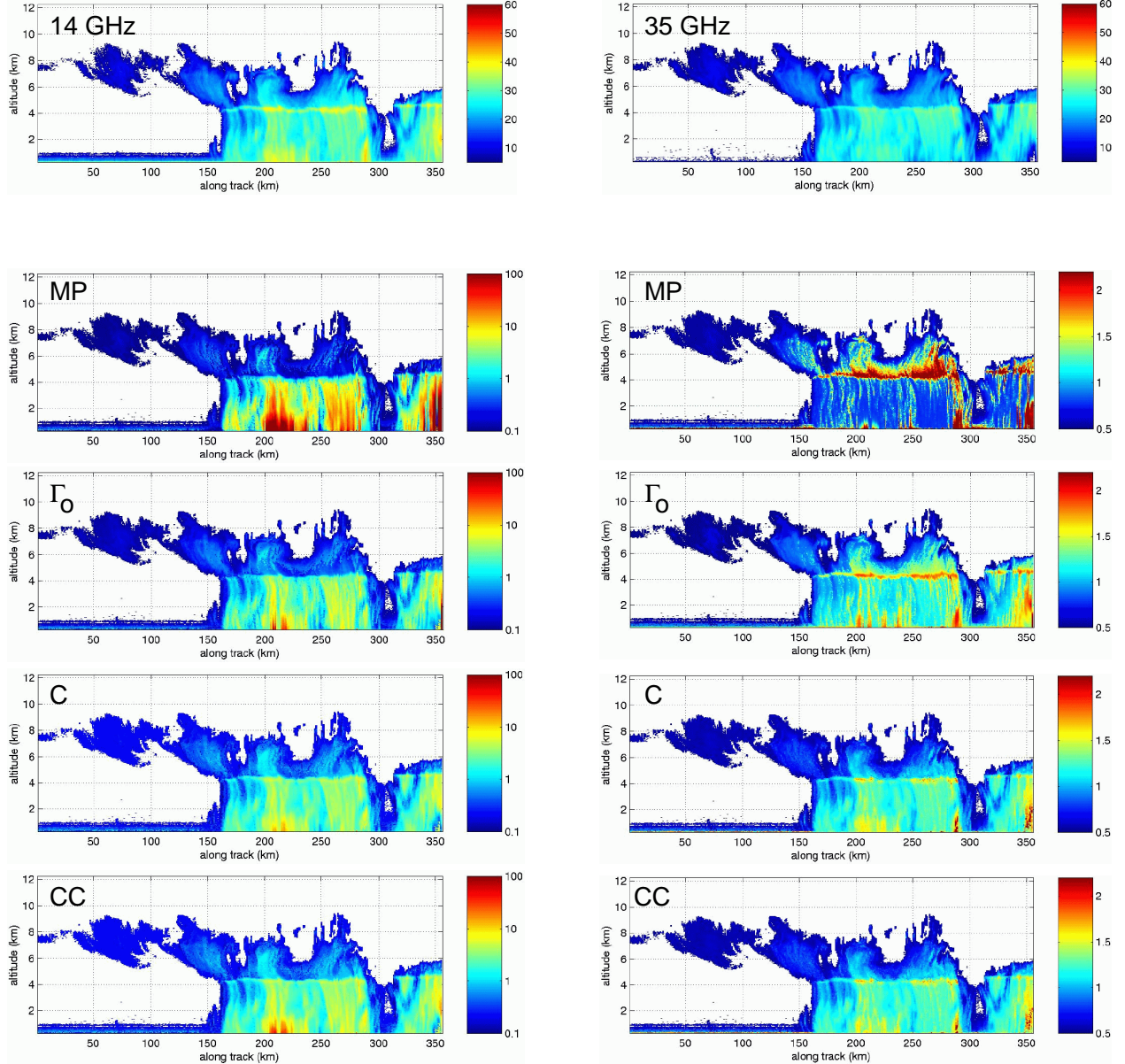


Fig. 5. Tropical Storm Gabrielle – measured radar reflectivities in dB (top panels), and retrieved rain rates R in mm/hr (left panels) and mass-weighted mean drop diameters D^* in mm (right panels).

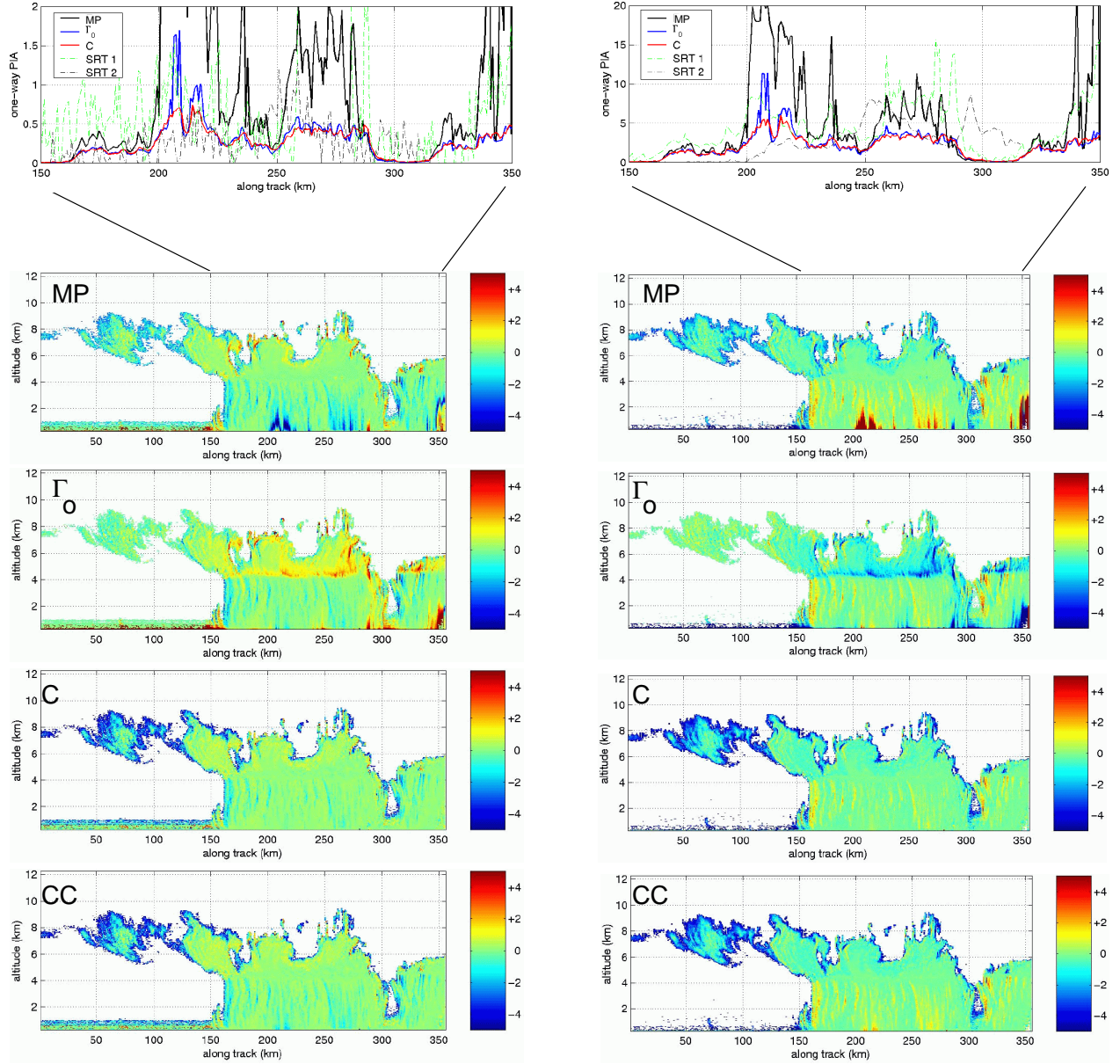


Fig. 6. *Tropical Storm Gabrielle – Path-Integrated Attenuations in dB (at 14 GHz in the top left panel, 35 GHz in the top right panel) and reflectivity errors $Z - Z_{\text{reconstructed}}$ in dB (at 14 GHz in the left panels, 35 GHz in the right panels).*

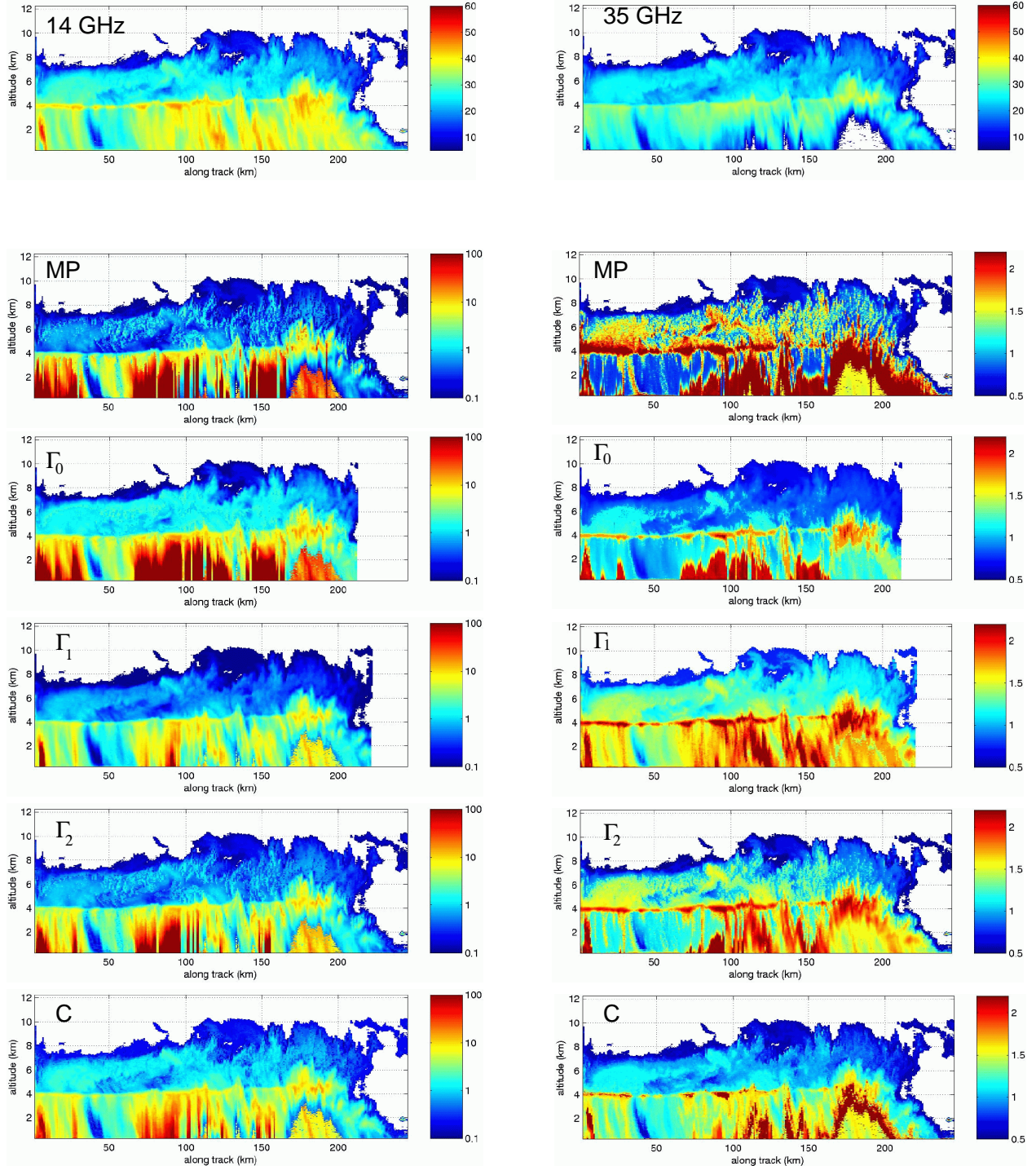


Fig. 7. Hurricane Humberto – measured radar reflectivities in dB (top panels), and retrieved rain rates R in mm/hr (left panels) and mass-weighted mean drop diameters D^* in mm (right panels).

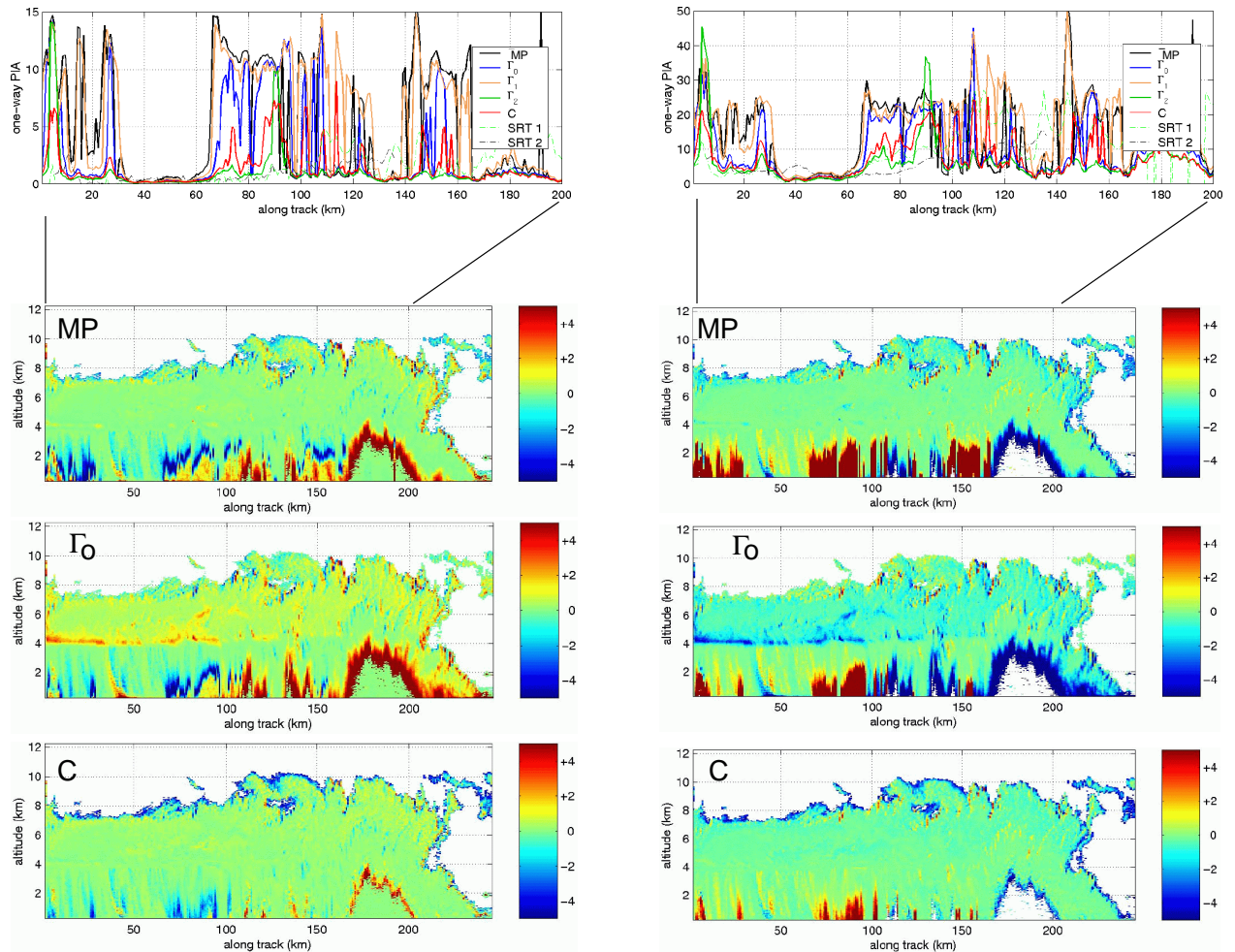


Fig. 8. Hurricane Humberto – Path-Integrated Attenuations in dB (at 14 GHz in the top left panel, 35 GHz in the top right panel) and reflectivity errors $Z - Z_{\text{reconstructed}}$ in dB (at 14 GHz in the left panels, 35 GHz in the right panels).

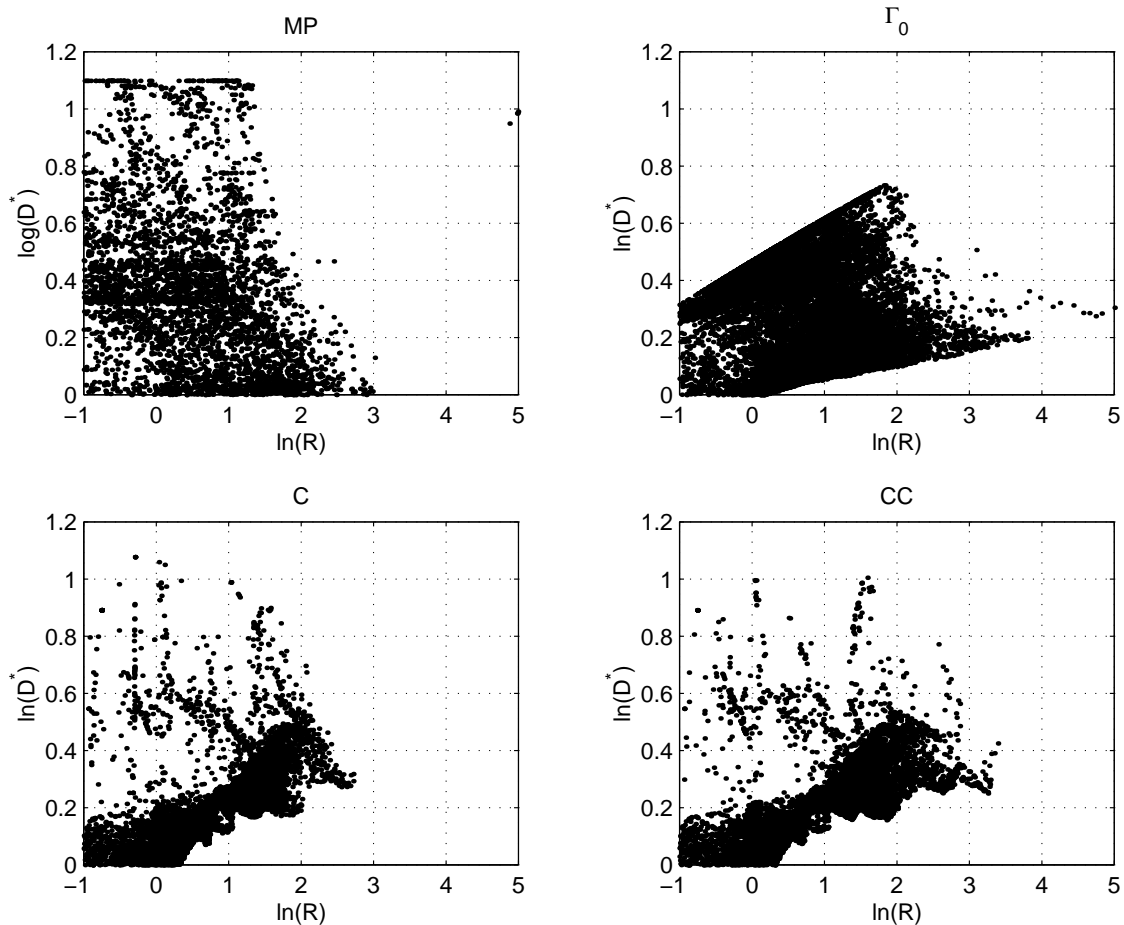


Fig. 9. Correlations between R and D^* in the case of Gabrielle.

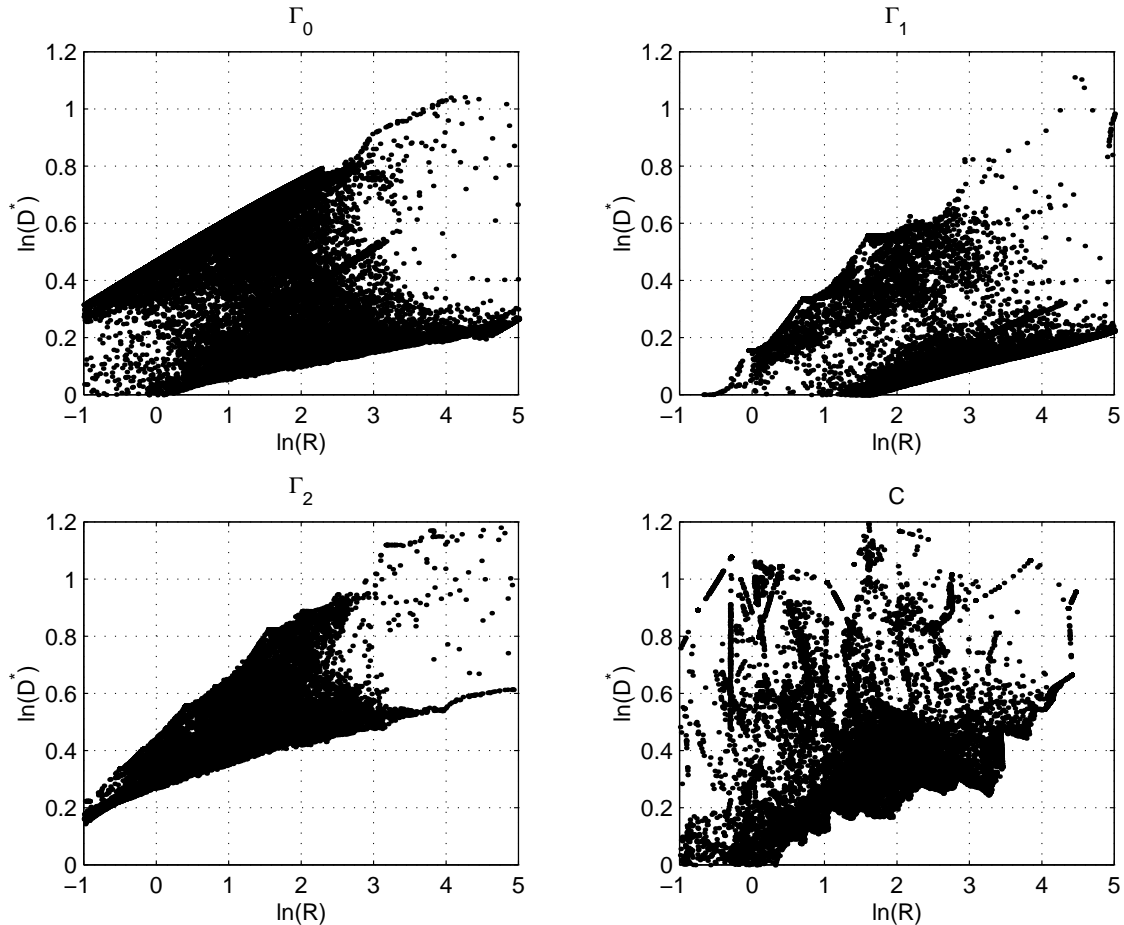


Fig. 10. Correlations between R and D^* in the case of Humberto.